

---

# Temporal Convolutional Network Based Trunk Muscle Signal Decoding for Exoskeleton Control

BIOE97051 MEng Biomedical Engineering Individual Project  
Final Report

---

Balint Karoly Hodossy  
*Imperial College London*  
*Department of Bioengineering*

CID: 01207299  
bkh16@ic.ac.uk  
Word Count: 5646

## Abstract

The main limitations of existing control strategies for exoskeletons are the lack of intuitive voluntary inputs, and slow speeds due to inaccurate predictions. Surface electromyography (sEMG) is a well established signal used to address similar limitations in related devices. However, many patients who could benefit greatly from exoskeletons have reduced, spastic or no muscle activity in their lower limbs. This project proposes a feed-forward Temporal Convolution Network model to regress lower limb kinematics in the sagittal plane from sEMG recorded from of trunk muscles. The model is constructed with 5 healthy subjects and evaluated in simulation targeting walking, sitting and stair climbing. The results show task specific models accurately predict joint angles in motion at a mean accuracy of  $R^2 = 0.86$  for the hip,  $R^2 = 0.90$  for the knee and  $R^2 = 0.61$  for the ankle. Preprocessing steps to remove electrocardiogram corruption and the use cases of movement and gait parameter classification are also considered.

## 1. Introduction

The loss of motor control in the legs drastically redefines not only mobility, but also how someone can take part in society. Paraplegia's main causes, stroke and spinal cord injury (SCI) [1], often require a sudden and unexpected change of lifestyle. Every year approximately 350 000 new people are affected by SCIs alone, leading to decreased rates of school enrolment and increased rates of unemployment and depression[2].

Patients most commonly rely on powered or self-propelled wheelchairs as a means of everyday transportation. These devices require accessible environments (e.g. stair alternatives) to function efficiently. Furthermore, due to a lack of movement in the lower body, a series of secondary condi-

tions (e.g. deep vein thrombosis, osteoporosis and pressure ulcers) are associated with paraplegia, increasing the severity of the condition [2]. A powered exoskeleton avoids these limitations of the wheelchair, addressing needs of SCI patients by restoring ambulation. This in turn can facilitate improvement in their top priorities, such as personal relationships, health, employability and access to services [3].

Commercially available exoskeletons have yet to realise their potential impact. While two of the main limiting factors are availability and affordability, some early user reactions suggest patient expectations need to be met by the technology before widespread adoption. There is evidence that if these needs are not matched initially, users may quickly disregard the device [4]. Key aspirations identified include an intuitive and natural control scheme that results in inconspicuous movement at convenient speeds [5]. Another is proportional control (opposed to on-off control, as defined by Fougnier et al.), which enables users to fine tune their gait for varying environments[6]. Satisfying these could mitigate the high abandonment ratio associated with assistive technology and mobility aids, and confirm that exoskeletons are a worthwhile alternative or complement to wheelchairs [7][8].

This project demonstrates a voluntary and proportional surface electromyography (sEMG) control model of joint kinematics and gait parameters, targeting a six degrees of freedom (DoF) Hip-Knee-Ankle exoskeleton, such as the Tech-aid Exo-H3 [9]. Five types of movement are considered in that are essential for day-to-day activities: sitting down, standing up, walking, stair ascension and stair descension. This selection was inspired by the stages of the Powered Exoskeleton Race of Cybathlon 2020, as this project is part of Imperial College's participation in the event [10][11].

## 2. Literature Review

Myoelectric signals have been central in the study of prosthesis/orthosis control for over 60 years as a form of non-invasive brain-computer interface (BCI) [12]. BCI based control strategies is an area of study identified as being key for the development of exoskeletons [13]. This is especially true in the case of paraplegia patients for whom BCIs could complement the roster of viable strategies, which is currently composed of predefined motions (e.g. selected from a wrist-pad controller) and biomechanical models (e.g. based on centre of mass) [14].

The challenge of sEMG based exoskeleton control for a user with loss of motor function in their legs, is that the intended leg muscle activity needs to be inferred from the signals of other remaining, still active muscles involved in the movement. This makes control schemes that rely on a user-specific Hill-type-musculoskeletal model to directly estimate torque in the legs unfeasible, such as those designed for paresis patients [15].

Activation of the *multifidus*, internal and external oblique muscles, as well as the *erector spinae* muscle group has been shown to be connected to the different phases of the gait cycle [16][17]. However, the extent and more importantly, the specificity of the relation to walking for other trunk areas (e.g. *latissimus dorsi*) is not as clearly studied.

Lacking a direct, robust biomechanical model, predefined sEMG features can form the basis of classification or regression using machine learning methods such as support vector machines [18][19]. Examples of these features are signal envelope, variance, mean frequency, number of zero crossings and autoregressive or wavelet coefficients [20][21]. Alternatively, biomechanical models can be complemented with other regression methods such as neural networks (NNs) [22]. The highly coupled and non-linear nature of muscle contraction and limb movements, is the kind of problem deep learning techniques such as NNs were designed to understand.

High-density sEMG envelopes have been shown to be sufficient in simultaneously estimating proportional angles in 4 DoF for the wrist-arm complex [23]. A separate multi-layer perceptron structured NN is used for controlling each DoF using up to 26 input channels. However, a considerable drop in accuracy is noted in at least one of the DoFs if the number of channels is reduced.

To maintain high accuracy with a limited number of electrodes, the temporal and frequency domain context of the signal can supply the required information. Traditionally recurrent methods like long-short term memory (LSTM) networks are considered for causal problems such as this, and there have been successful applications of such architectures when combined with convolutional layers for es-

timating the position and orientation of the shoulder [24]. The convolutional part is responsible for identifying and extracting key features for pattern recognition over time, and the LSTM imparts the ability to allow the previously recognised states to affect the current one. Recently however, there have been successes of primarily convolutional, non-recurrent models called temporal convolutional networks (TCNs) outperforming recurrent ones in the field of gesture recognition, while achieving faster training times and predictions [25][26] [27][28]. This creates a motivation to see how they would adapt for regression.

A related field of computer science, procedural character animation also offers many successful techniques that are yet to be adapted for prosthesis and orthosis control. Phase-functioned neural networks for example produce smooth and robust real-time walking, running and stair climbing movements based on simple user guidance[29], and neural state machines shows virtual avatars adaptively interacting with the environment with complex motions, which could have key lessons in successfully navigating rough terrain and stairs of different dimensions [30].

### Research gaps identified

There is less literature coverage concerning the lower extremities, and by extension exoskeletons, than those regarding arms and hands. Similarly, BCI applications are generally more common for classification than regression in prior art. Furthermore during the review, no study was found trying to estimate leg movements from trunk muscle activation, the closest comparison being the estimation of hand kinematics from forearm signals. No applications of deep learning techniques (such as NNs) were found for sEMG based voluntary lower-limb exoskeleton control, which have shown significant success in an arm and shoulder context.

Another gap is the application of techniques from procedural character animation. Many methods are based in robust physics simulation engines, therefore there is a possibility these could transfer well to the real life [31][32].

Finally there has been a call for greater involvement of the end-users in a process of human centred design for exoskeletons [5][33].

## 3. Methods

The scope of the project and its place in the context of exoskeleton control is illustrated in Figure 1. The project implements a non-recurrent TCN model for regressing 8 channels of bipolar sEMG electrode signals to the hip, knee and ankle joint angles of the leg in the sagittal plane. The cases of level-surface walking, stair ascension, stair descention, sitting down and standing up (referred to as tasks from now on) are addressed separately, connected by an

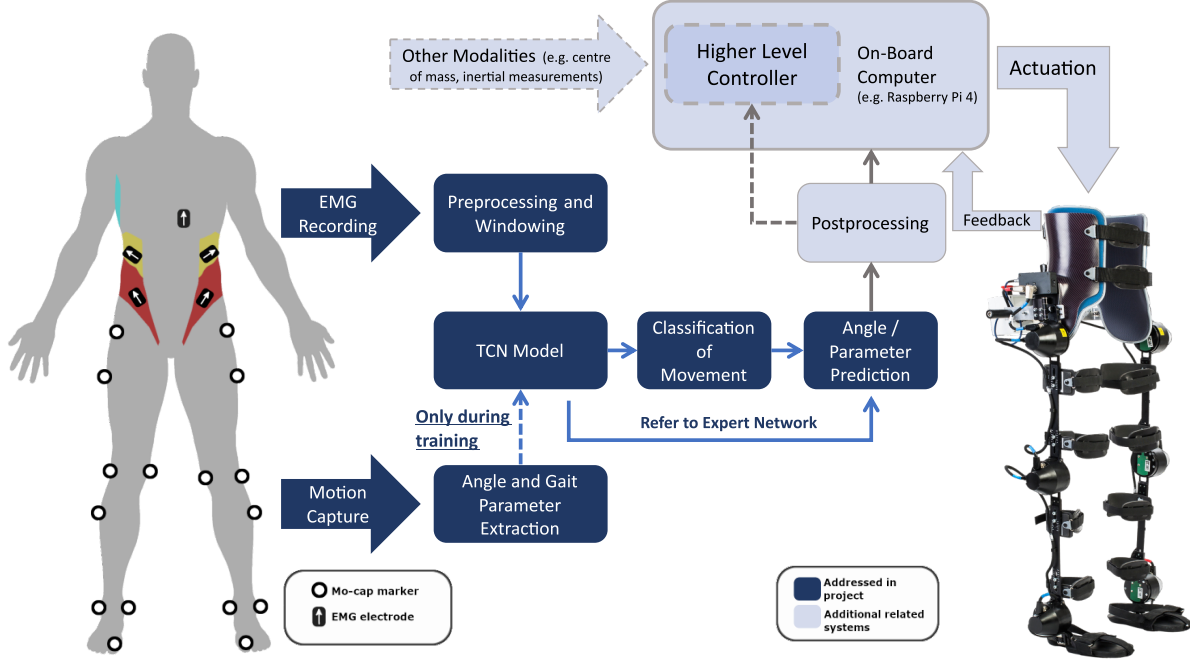


Figure 1. Flowchart of the application of this report’s methods for exoskeleton control. Segments in dark blue represent the scope of this project. Segments in light blue represent other aspects likely to be involved in an implementation of exoskeleton control. Exoskeleton image from Technaid [9].

initial task classifier step. Furthermore it is demonstrated that the model transfers well to a gait parameter prediction problem, and accepts inputs of sEMG features such as its spectrum. Models were built and trained using tensorflow’s Keras library in Python [34][35][36]. The report addresses the preprocessing and filtering of the sEMG data, as well the extraction of joint angles from motion capture data, based on recordings from 5 subjects.

### 3.1. Experimental Procedure

4 male subjects (subjects 1, 3, 4 and 5), and 1 female subject (subject 2) participated in the recording experiments. Based on preliminary results the last two subjects’ number of repetitions were increased from 20 walk, 8 sit, 8 stand, 10 stair ascend, 10 stair descend to 50, 25, 25, 25, 25 respectively. Half of walking and stair climbing recordings were started with the right, half with the left foot. Figure 2 shows the motion capture reflective marker locations and the electrode placements.

Reflective markers were placed on the following locations:

- Medial/lateral epicondyles of the knee and ankle
- Anterior superior iliac spines
- Sacrum

- Thighs and shanks, laterally
- Heels
- Proximal phalanges of the big toes

Muscle groups were identified via palpation, and electrodes were oriented parallel to their fibres. An additional electrode was placed under the pectoralis to collect a reference electrocardiogram (ECG) signal (see Figure 2).

The right side of the back was targeted with more electrodes for less ECG corruption. For the second group the *latissimus* electrode was moved to the left *trapezius* location, to also explore a setup more balanced between the left and right sides. The motion capture was made with a Vicon Motion Systems environment, synchronised with the Delsys Trigno wireless bipolar sEMG electrodes [37] [38].

### 3.2. Joint Angle and Gait Parameter Extraction

Interpolation of gaps in marker trajectories was performed using Vicon Nexus, via a mixture of cubic spline interpolation, cyclic interpolation and rigid body models, chosen on a case-by-case basis [38]. Knee and ankle joint centres were estimated as the midpoint between the corresponding epicondyle markers. Hip joint centres were approximated based on the anthropometric model of Vaughan [39]. The flexion-extension was defined based on the Joint Coordinate

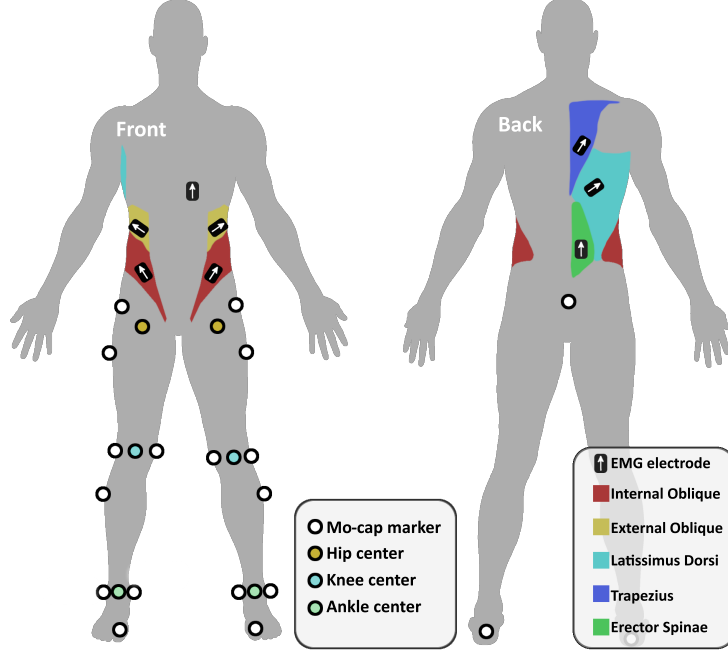


Figure 2. Recording setup for data collection, and angle extraction

System method of Grood and Suntay [40]; the coordinate systems used to calculate these angles are shown in Appendix A. Figure 3 presents resulting angles for the stair task.

To demonstrate the model transfers well to the related problems of step side and stride length classification, relevant gait parameters were extracted (Figure 4). The step side is defined as the leg in swing phase, determined based on the heel markers' velocity. This is classified as no-step, left stride and right stride. Stride length is defined as the maximum distance between heels during a given stride, projected onto the frontal axis, and is classified as no-step, half step, and full stride. No-step classes require the network to determine the onset of the first and end of the last step's parameters.

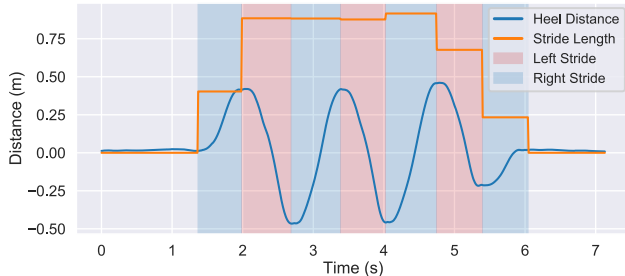


Figure 4. The derivation of gait parameters that form the classes for secondary model. Half step is performed at start and end of cycle.

### 3.3. sEMG Data Generation and Preprocessing

The joint angles were resampled with linear interpolation from 100 Hz to the sEMG's 2000 Hz, and paired with windows of sEMG data in a one-sample-ahead prediction setup. 0.5 second windows of the 8 normalised electrode channels were sampled from the recordings at a 10 ms stride (20 samples) as the input to the networks. For the sitting task the sampling stride between windows was reduced to 2.5 ms (5 samples), due to smaller datasets.

Since all training was performed on consumer-grade hardware, being memory efficient was necessary in order to train with windows longer than 100 ms. Due to the overlapping regions there is a high degree of redundancy in the input data. This was addressed with a custom implementation of the DataGenerator application programming interface of Keras, which samples windows of the sEMG signal and supplies them to the network as it requests them, avoiding duplicate data in memory.

Longer windows involve more computations per prediction, and longer persistence of signal artifacts/noise spikes, should they occur. However, if window sizes are reduced high spikes of error were observed, correlated with heartbeats, as the model has less information without ECG corruption to make predictions with. A comparison is seen in Appendix B. Therefore it is of interest to reduce the extent of ECG corruption in the recorded channels, which can be identified in both the time series and the spectrum of the

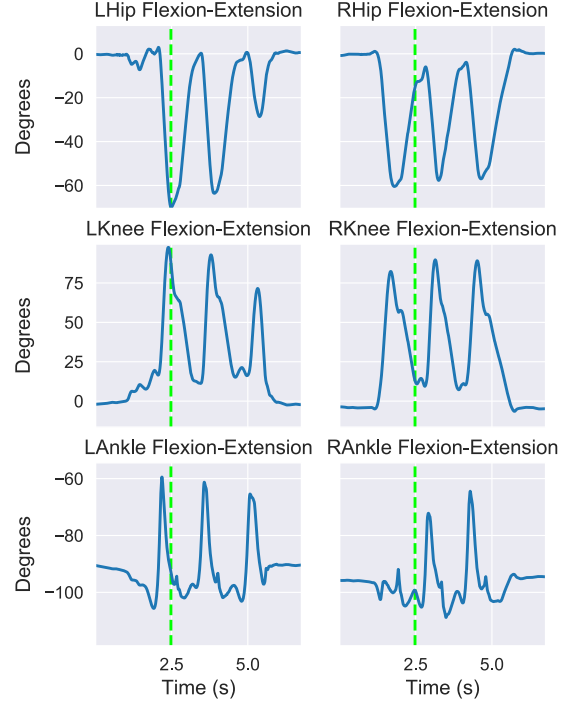
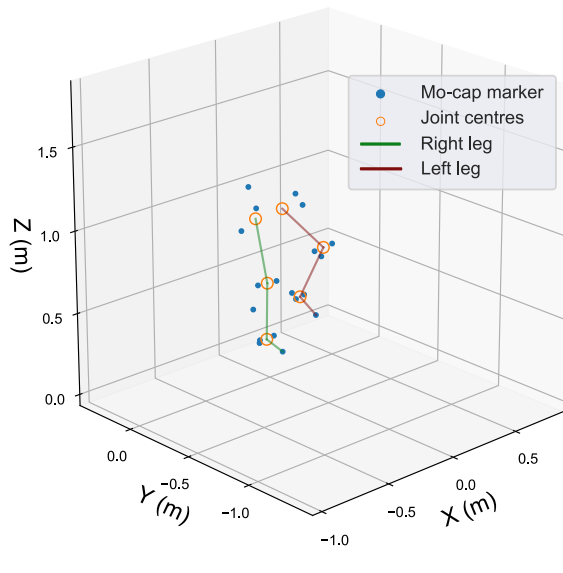


Figure 3. Example marker positions and joint angles during stair climbing. The dashed green line marks the corresponding angles in time to the 3D plot on the left.

sEMG channels (Figure 5). This could enable the use of shorter windows.

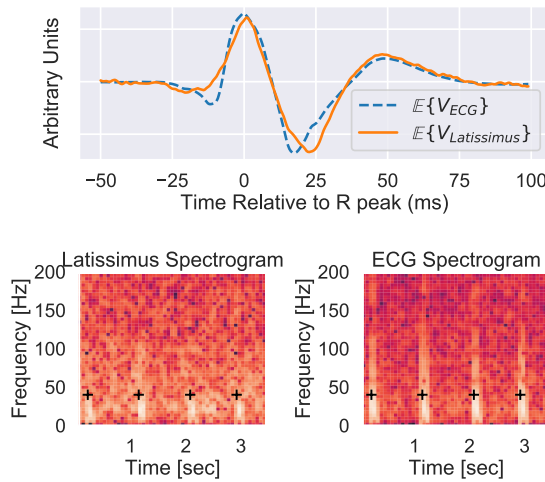


Figure 5. ECG corruption in time-series and spectrum. Time series plot is the average latissimus' and ECG activity for subject 5, aligned based on the position of the R peak. In the spectrum, + marks the same positions in time for comparison. Note the overlapping spectrum, and that greatest frequency components in latissimus is due to ECG corruption

3 methods of addressing ECG corruption are compared with a control case for the walking task:

1. 4<sup>th</sup> order causal Butterworth high-pass filter, with cut-off frequency of 35 Hz. Parameters were chosen based on existing literature on their effects on signal-to-noise ratio (SNR), and inspection of spectrograms [41][42].
2. Adaptive noise cancellation, with the computationally cheap Normalised Least Mean Squares (NLMS) algorithm. This is a simple algorithm to begin investigation in this area with, and it has been applied in a similar context with some success [43]. Filter order 4 was chosen based on average QRS window's partial autocorrelation (Appendix D).
3. Supplying the ECG reference signal unprocessed to the network. It is hypothesised that the network might learn to decorrelate the ECG signal due to its consistent shape, and supplying a clear reference could help this process.

To quantify the quality of recordings the following metrics are defined to estimate SNR:

1. *Early step activity*. This is the root-mean-square (RMS) of a channels voltage during the first half of each step.

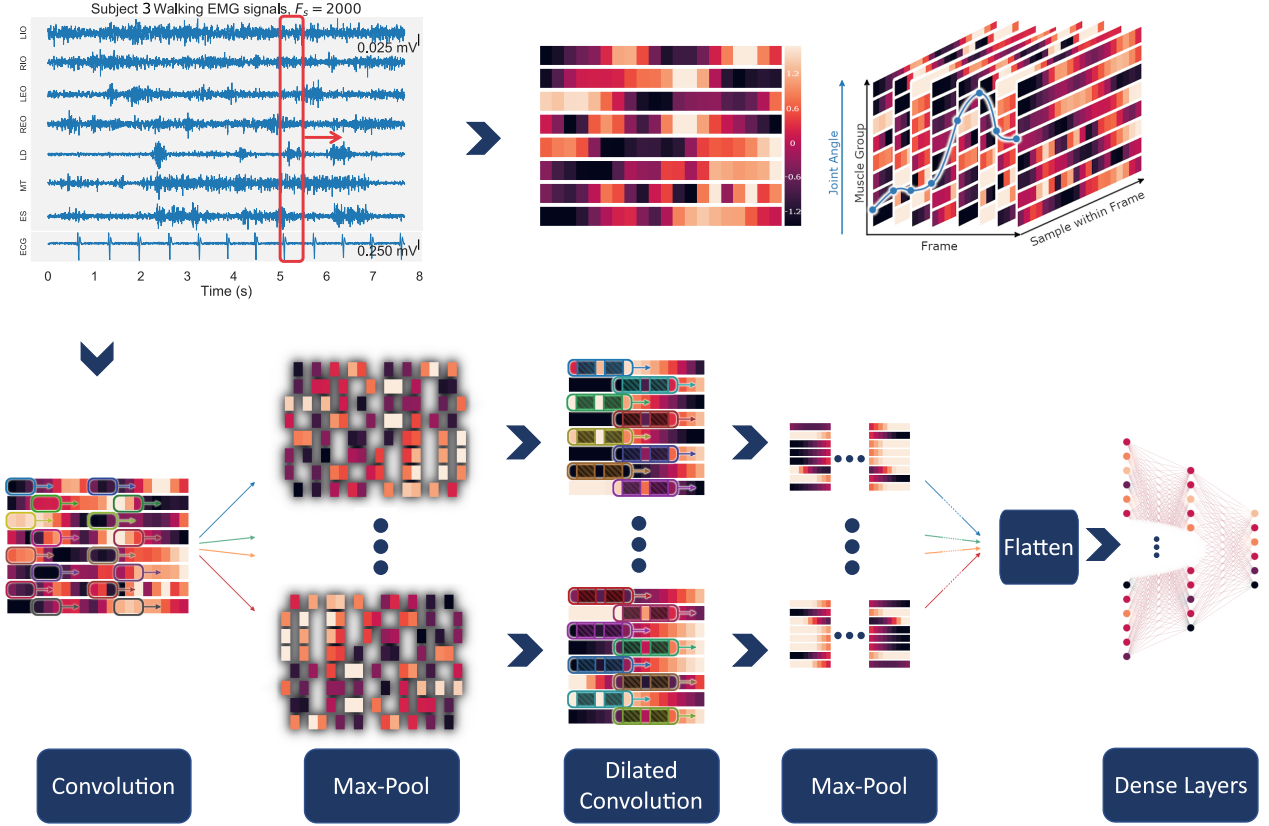


*Figure 6.* Chart outlining model structure. *Top Row:* Windowing of sEMG data, and pairing windows up with joint angle values. *Bottom Row:* Structure of the network. The convolutional filters increase the dimensionality in feature-space, while max-pooling reduces it in the time-domain.

2. *QRS activity.* RMS during heartbeats, defined as a 50 ms before and 100 ms after each R peak, based on the average length of the QRS complex [44].
3. *Background activity.* RMS in regions not included in either previous metrics.

The background SNR is then quantified as  $SNR_{bg} = \frac{1}{3}$ , and the ECG SNR is defined as  $SNR_{ECG} = \frac{1}{2}$ .

### 3.4. Neural Network Models

The prediction model can be separated into two halves: the decoding adaptive feature extraction phase consisting of convolutional layers, and the inference phase with densely connected layers (Figure 6).

The feature extraction is performed channel-wise, with no connections between nodes of different muscle signals until the densely connected layers. This leads to better generalisation, as the filters must learn to extract meaningful features tailored for their channel, while traditional convolutional

layers of the same length would have higher degrees of freedom in filter weights, which could lead to overfitting on the patterns of the training set. Secondary feature extraction is performed with dilated filters, increasing their field of view, allowing the network to capture longer term patterns as well without loosing resolution [25]. These layers all use the Rectified Linear Unit (ReLU) activation, as this is the most computationally intensive parts of the network, and the sparsity of ReLU layers leads to faster updates. Max-pooling is used to reduce the dimensionality of the data, as well as to increase the field of view. To connect these features with the dense layers, nodes are flattened into a single vector.

Out of different regularisation methods, dropout layers were found to be the most effective, and are placed between every dense layer with a dropout rate of 0.5. This high dropout rate across the dense layers is facilitated with the use of Scaled Exponential Linear Unit activation, which also allows the use of better performing deeper networks without overfitting [45]. The final layer has linear activation and mean square error loss for angle regression (adapting to mean and variance of the signal automatically), or softmax activation

and categorical cross-entropy loss for classification problems. Classification networks use shallower and narrower dense layers, necessitated by the limited complexity of these problems.

Four applications of this network have been investigated:

1. *Angle regression for all 5 tasks.* Due to the periodic and coordinated nature of the gait cycle, the joint angles have high statistical dependence on each others' values. Therefore the ideal features extracted from the inputs, upon which predictions are made are likely to be related for all channels. As such, the angle regression model predicts all six degrees of freedom at once. This significantly decreases the computational load for an exoskeleton's control, when compared to prediction with a group of joint-expert networks. Since the network is feed-forward and open-loop, it is unable to simply memorise the average kinematics during the tasks and must rely entirely on sEMG recordings.
2. *Task classification.* The walking and stair datasets were reduced in an attempt to make samples more stratified. While sitting tasks were recorded the same amount of times, the shorter recordings resulted sitting/standing up classes being less likely to occur during classification otherwise.
3. *Gait parameter classification.* The feature extraction layers can be copied from the angle regressor, and transferred to related problems, such as classifying stride side or length. This technique has yielded networks that learn much faster and can perform with higher accuracy in other areas of machine learning [46]. This gives motivation to see if sEMG features learnt by the angle regressor could be reused by other systems. To test this the filters of convolutional layers trained for a given subject on the same train-test data split replaced the initial layers of these gait parameter classifiers and their training were turned off.
4. *Regression with alternative inputs.* Finally, it is shown that this type of model is able to learn and predict using alternative sEMG derived features, such as its spectrum. The iterative DFT-CLMS algorithm was used to calculate the spectrum, with a leakage term to localise estimates in time [47][48].

These models are evaluated using 5-fold cross-validation. The validation split is performed between recordings to ensure statistical independence of splits. Early stopping is implemented, therefore training is stopped if validation loss has not improved for more than 25 epochs, and the model with the best generalisation is evaluated. The main body of the results use the ECG reference channel as heartbeat corruption attenuation approach. When this approach is

compared to other ECG preprocessing methods, including the control case, the input length of models is reduced to 200 ms, as ECG corruption is most prominent in shorter windows.

## 4. Results

### 4.1. Angle regressor

The task-specific models successfully learned to predict the 6 joint's kinematics of the tasks for all but one subject. No significant difference was found between errors of the left and right sides, therefore their average is used in the further analysis. The mean coefficient of determination was 0.86, 0.90 and 0.61 for hip, knee and ankle predictions respectively across all subjects and tasks (with one outlier case removed, to be addressed). The results of the cross-validation for the angle regression are presented in Figure 8, and Figure 7 shows a sample prediction for the walking task.

Before comparisons are made, the missing elements from the charts are addressed. One of Subject 1's marker was obscured during the sitting task, making angle calculations for the ankle impossible, as such these recordings were excluded from the analysis. Subject 1's walking model just regressed to the mean (i.e.  $R^2 = 0$ ), possibly due to poor electrode fitting.  $SNR_{bg}$  was found to be double for the stair recordings of Subject 1 when compared to their walking recordings (4.54 vs 2.13), reinforcing the hypothesis of poor electrode fitting. This highlights this model's requirement of consistent, good quality signals. For this reason Subject 1 is removed from all further analysis involving either sitting or walking tasks due to being a clear outlier.

#### 4.1.1. COMMON PATTERNS

The results reflect some of the datasets characteristics of interest, which include types of errors shared across subjects. Future work could be directed by trying to address these specifically.

Subject 3 adjusted their footing during sitting tasks twice. Based on the distance of the heels from the base of the chair the ankle angles are biased for the whole motion. As a result there is particularly poor performance in the ankle joint, and high variance based on which foot positions are included in the training set. In the case of standing up the  $R^2$  was negative. This phenomenon could be shared to some degree by other subjects, causing the low  $R^2$  values of ankles, and errors are magnified by the joint's relatively low range of motion. This is not considered to be an outlier in the results, but rather as one of the most important limitations of the system. The open-loop nature of the model is an important factor in this prediction error; using feedback about the exoskeleton's current state would be crucial to address it.

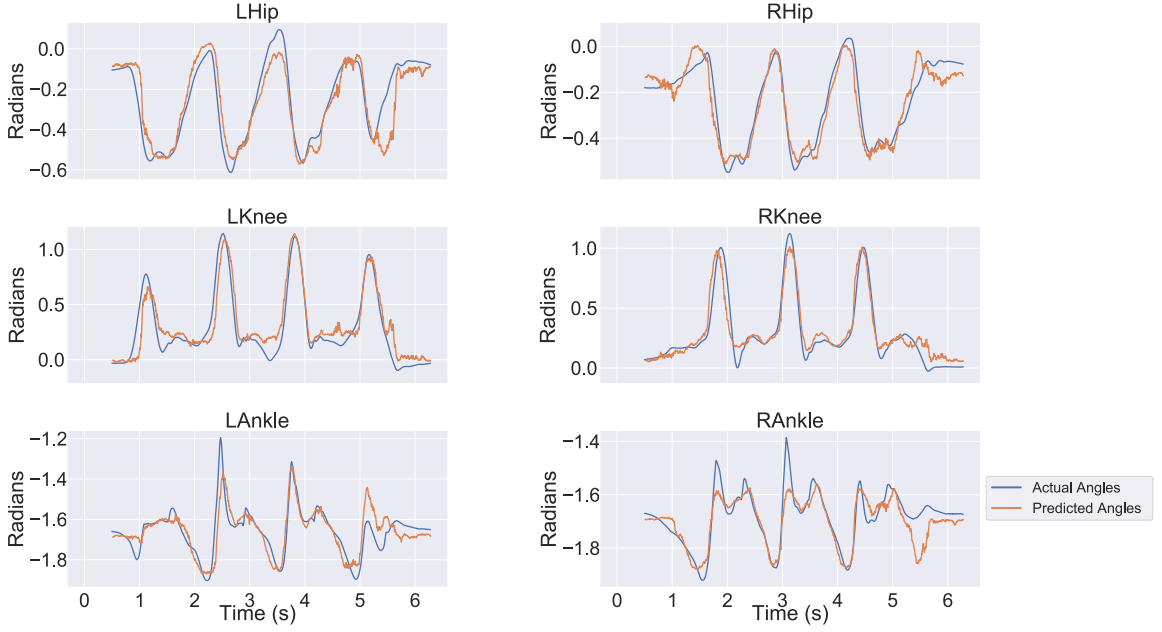


Figure 7. Walking Angles for Subject 2. As example postprocessing, a 10ms long causal moving average filter is applied.

The sitting task also suffers from another common problem. Due to the similarities of the muscle signals in the two resting states (fully standing or sitting), the greatest errors occur when the movement is in either of these states. One of Subject 2's sitting down recordings contained a longer sequence of standing, which lead to greater error of the model when validated on it. This is observable on the larger variability of this subject sitting down performance.

Standing up predictions likely outperform sitting down (comparing  $R^2$  values) due to greater range of motion in the hips, and due to muscle activity slightly preceding the motion since standing up involves first bending forward slightly.

When ascending the staircase the hips are more involved as we overshoot the step's height (example in Appendix C), while the ankle is used to compensate for the height decrease while descending (1.6 times greater range of motion in ankles for descension than in ascension). These characteristics are reflected in the  $R^2$  values of the hip and ankle when comparing the two tasks. It is of particular interest that the increased range of motion resulted in increase in both RMS error and  $R^2$ , suggesting the information in the extra muscle activity elicited by the greater movement more than counterbalances the relative heightened error.

#### 4.1.2. COMPARISON WITH RELATED MODELS

To validate our hypothesis that a channel-wise separate layers improves model prediction accuracy, we compared our

proposed model with one with the same number of traditional convolutional filters. This benchmark network's mean error across subjects with the walking dataset was  $10.4^\circ$ , significantly worse than the channel-wise model in a paired t-test at  $p = 0.0077$

When the model was trained on all 5 tasks at once, the mean performance dropped significantly ( $R^2_{\text{hip}} = 0.77$ ,  $R^2_{\text{knee}} = 0.79$ ,  $R^2_{\text{ankle}} = 0.42$ ). The mean  $R^2$  values across subjects for each 6 angles was compared in a t-test paired for joints,  $p = 0.009$ . This decrease was also present in subjects 4 and 5, therefore it was not primarily caused by the electrode refitting of subjects 2 and 3.

## 4.2. Task Classifier

Mean validation accuracy was 93%, 96%, 90% and 73% for subjects 2, 3, 4 and 5 respectively for distinguishing between the five tasks. However, it must be considered that subjects 2 and 3 had electrodes refitted between at least 2 tasks since their recordings took part on two occasions. While the positions of the electrodes were marked on subjects, the nature of the interface could have changed for them. Signal properties such as SNR, variance and noise components could have changed between electrode fittings. If this is the case, a neural network is very likely to exploit this fact, which could explain why the accuracy is higher for subjects 2 and 3, therefore their results should not be taken at face value. For example the largest error was in the sitting task's classification (5 times as much as in the walking task), suggesting

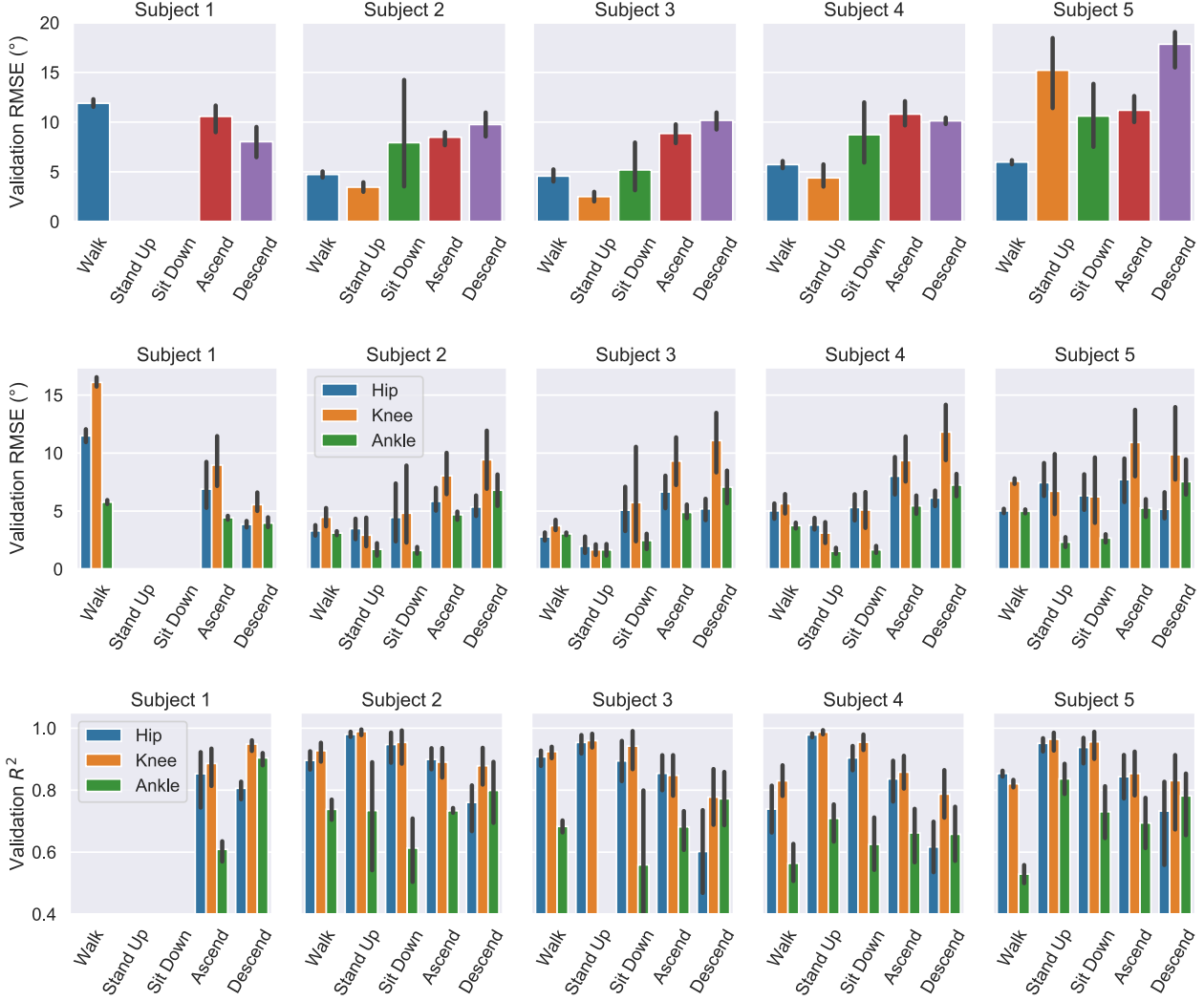


**Figure 8.** Angle regression model’s performance metrics. *Top row:* Root of the mean validation squared errors across angles summarising performance. *Middle row:* Analysis is separated in terms of angles beyond this point. Average error across a given trial for each subject. Values of left and right sides are averaged together within each fold of the crossvalidation. *Bottom row:* Coefficient of determination / scaled accuracy of given angle and task. Note y axis starting at 0.4. Error bars represent standard error of the mean.

that the stratification strategy was ill suited for a fair training and evaluation (see Figure 9). Surprisingly, when training was performed using the entire dataset, without reducing the proportion of walking and stair recordings, the accuracy increased even for the sitting tasks (prediction error for sitting classes of Subject 5 halved). For these reasons the accuracy values should be interpreted as indication that a task classification system could at least be partially based on a TCN based prediction. Introducing recurrency, feedback from the exoskeleton or encoder-decoder architectures are all candidate approaches to increase the robustness and reliability of the classifier. They all promote making connections between past states and the current ones, resulting in less probability of unlikely combinations (e.g. we rarely transition from sitting down straight into stair climbing).

#### 4.3. ECG filtering

Maintaining stability of the NLMS filter was problematic with linear activation due to the spiking nature of the ECG and electromyography (EMG) signal; this was addressed with a switching to ‘tanh’ activation which was consistently robust against outliers. Example performance is shown in Appendix D.

The 5 fold cross-validation results of the models with the different preprocessing methods were analysed with a repeated measures ANOVA of the  $R^2$  values, showing no significant difference. If subjects are inspected individually, providing the ECG channel to the model yielded considerable improvements in subjects 2 and 5, for whom the  $SNR_{ECG}$  was the lowest. However further testing with more partici-

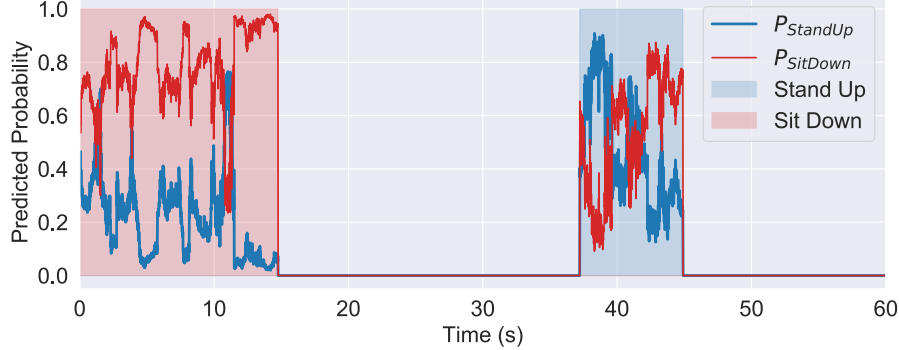


*Figure 9.* The classifier network’s classifications on the validation sitting recordings, which performed the worst. Subject 4’s results are shown. Shaded areas show the true classification. All validation recordings of the two tasks are concatenated with other tasks to show absence false positives in cases of walking and stair tasks. Sitting down is better predicted, which at least partially influenced by being better represented due to the longer nature of movement.

pants should be conducted before making conclusions.

#### 4.4. Transfer Learning

Step side and stride length classification for the walking task performed across subjects at a mean accuracy of 86.8% and 77.1% respectively. While transferring the pretrained layers yielded no significant improvements in performance, the training time was one fifth using them at no cost to accuracy. These results not only suggest that a TCN architecture can be used to extract information regarding gait parameters, but that the learned features can be reused in related problems.

#### 4.5. Learning from alternative sEMG features

The iterative spectrum estimation could reliably produce frequency features corresponding to the events of the gait cycle, shown in Figure 17 in Appendix E. It was observed that the greater the leakage factor, the more localised are the estimates in time, but more spread out in frequency. This can be thought of as a manifestation of the uncertainty principle.

Due to the much longer training times involved, running comprehensive cross validation for this section was outside the scope of this project. Appendix E shows an example prediction of Subject 2 for comparison with Figure 7. Note the smoother predictions, but also the much more pronounced ECG corruption.

### 5. Discussion

The project addressed a wide range of concepts regarding exoskeleton control based on trunk muscle signal decoding with an open-loop TCN model. The work presented should be considered as initial exploration of the application of these deep learning methods to the trunk muscle signals,

revealing research areas of interest to address with future work. Techniques and methods were applied from different but related topics such as gesture classification. These were found to be appropriate to establish a meaningful connection between trunk muscle signals and crucial everyday tasks such as walking, sitting down and stair climbing. The model was cross-validated for these movements and its performance was quantified for different joint types, which will serve as a baseline to compare future modified models with.

Common types of error, including inability to predict ankle angle offset, and ECG corruption were identified. Different approaches to address the latter were proposed and implemented. It was demonstrated that the TCN architecture is compatible with different sEMG derived inputs. The adaptive features it extracts are applicable to various functions related to exoskeleton control, and are reusable in a transfer learning sense. These findings indicate that TCN models could be considered as building blocks in a higher level controller. Furthermore, the transfer learning capability of this model may prove to be essential in real life implementations; due to the difficulty involved with collecting motion data with patients, feature extraction layers pretrained on a large dataset could be appended to untrained inference layers which adapt to their users in a shorter data collection/training phase.

The model was able to regress to multiple DoFs at once, saving computational complexity. While some key network elements were identified (e.g. dropout layers and Scaled Exponential Linear Unit activation) no in-depth comparison was made between different window lengths and other network parameters. This is due to high type 1 error associated with train-test split based validation on limited datasets [49]. As such the statistical tests should therefore be primarily relied on as heuristics. However, two key findings, as suggested by the results so far, are:

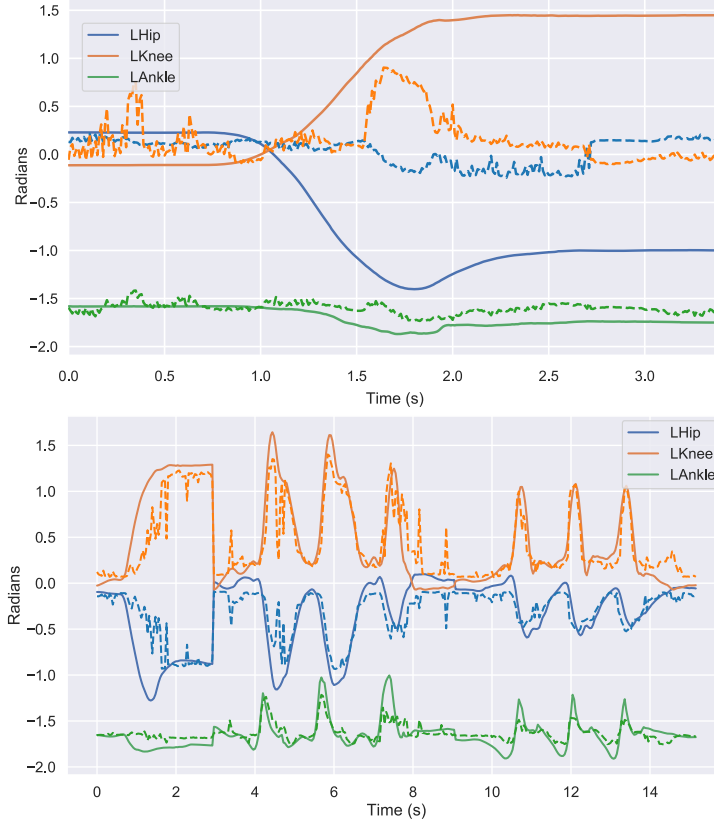


*Figure 10.* Top figure: Subject 5’s walk specific model tested on sitting data. Bottom figure: Subject 2’s generic model evaluated on sitting down, stair ascension and walking tasks. Dashed lines are predictions, solid lines are actual values

1. Channel-wise separate filters perform better than a network with the same amount of traditional convolutional filters.
2. Task agnostic general models, despite having more recordings, performed worse.

The second finding makes the assumption of a sufficiently reliable classifying step, in absence of which general models should be used. A further implication is that the task specific networks reach their high accuracy by exploiting the highly stereotyped nature of their given task, sacrificing accuracy in other tasks. Figure 10 show the poor generalisation of walking model when tested on sitting data. Combined with the fact that the general model performs on average at  $R^2 > 0.70$  for the hip and knee, this shows that the TCN model was able to adapt to different motions simultaneously, but generalises badly to types of motions outside their dataset. Therefore, for a static model that performs no learning once it is online, the training data needs to be from a comprehensive set of environments and movement variations. It is possible that given a sufficient training set and improvements to the network’s design, general networks

could perform as well as task specific ones, eliminating the need for a classification stage.

The metrics of these models can be contrasted with the results of existing implementations of sEMG based device control. Firstly a comparison can be made with exoskeleton control strategy based on muscle models using sEMG from the legs of healthy and paresis patient subjects performed with root-mean-square error (RMSE) ( $\sim 7$  degrees in knee,  $\sim 1.6$  degrees for ankle) comparable to our TCN model’s results [15]. In a second comparison, our  $R^2$  values were on the level of a high-density sEMG envelope derived feed-forward NN controller’s ( $\sim 0.86\text{--}0.93$ ), designed for arm prostheses [23]. These two comparisons show that the temporal context of a limited number of trunk muscle signals can supply the missing information that would otherwise be obtained from strongly correlated signals of the leg or high-density measurements. However, it must be noted that until tested, the behaviour and performance of a real life implementation is hard to predict, and might not be straightforward.

The network’s size and complexity was chosen so an implementation in real life hardware would be feasible. Subject

to optimisation of the prediction process, the number of floating point operations are on the order of  $10^6$ . Consumer-grade on-board computers such as the Raspberry Pi 4 can manage operations on the order of  $10^9$  per second. This makes predictions on the proposed one-sample-ahead level feasible. To limit the computational power that prediction needs, the network could be retrained to predict further ahead in time, as it is not necessary to make predictions every millisecond. While early tests suggest greatly increasing this delay can cause errors at the end of the gait cycle, it could also enable the use of non-causal postprocessing. Post-processing techniques such as moving average and median filtering will be crucial to decrease variability and attenuate spikes of error, but are also necessary to mitigate potential safety risks for users by enforcing limits on angle, angular velocity and torque.

A series of future directions have been identified:

- Analysis should be to quantify which muscle group channels provide the most information, to enable the reduction of the required number of channels.
- The dataset needs to be extended, with different variations of gait parameters (e.g. speed or step length). More reflective markers are needed to facilitate better gap interpolation. Repetitions of tasks need to be scaled for their duration, range of motion and the subject's height. This could facilitate multi-subject models, or improve the performance of task-general models. Learning transfer between subjects should be investigated.
- Due to the ankle's poor performance, the possibility of replacing this part of the regression with a model based on the other two joint's angles should be investigated.
- Methods to transition between classifications, such as a maximum likelihood estimation solution need to be investigated.
- Hyperparameter optimisation should be pursued to determine well performing architectures. Recurrent and closed loop elements are also high priority areas to investigate. Encoder-Decoder versions of the TCN have been shown to have good stability properties and should be evaluated for this application [26].
- Connecting the TCN to a Reinforcement Learning agent is a promising opportunity to benefit from the stability, flexibility and robustness of these motion synthesizers. This method could enable adaptation to environments and tasks of properties different than the ones observed in the dataset, which is one of the greatest limitation of the model [50][30][51].

## 6. Conclusions

TCN is a promising and versatile method for extracting information of trunk-muscle signals, making it a valuable source of information for the purpose of exoskeleton control. This study demonstrated its ability to regress to angles, classify movements and classify gait parameters across different tasks and subjects. High performance was reached with the hip and knee. This method is a promising candidate to be used in multi-modal model of ambulation.

## Acknowledgements

I would like to express my appreciation to my supervisors, Professor Dario Farina, Dr Deren Yusuf Barsakcioglu, and Dr Hsien-Yung Huang for their advice, guidance and support throughout my project. I would like to thank Professor Anthony Bull for making the equipment of his laboratory available for the project. I also wish to thank Hristo Dimitrov for his help with the motion capture software, and Dr Moon Ki Jung for providing the script for reading .c3d files with python.

## References

- [1] Brian S Armour, Elizabeth A Courtney-Long, Michael H Fox, Heidi Fredine, and Anthony Cahill. Prevalence and causes of paralysis—united states, 2013. *American journal of public health*, 106(10):1855–1857, 2016.
- [2] World Health Organization. Spinal cord injury. <https://www.who.int/news-room/fact-sheets/detail/spinal-cord-injury/>, 2013. [Online; accessed 10-Jan-2020].
- [3] Lisa A Simpson, Janice J Eng, Jane TC Hsieh, Wolfe, and Dalton L the Spinal Cord Injury Rehabilitation Evidence (SCIRE) Research Team. The health and life priorities of individuals with spinal cord injury: a systematic review. *Journal of neurotrauma*, 29(8):1548–1555, 2012.
- [4] Syed Ghulam Sarwar Shah, Ian Robinson, and Sarmad Al-Shawi. Developing medical device technologies from users' perspectives: a theoretical framework for involving users in the development process. *International journal of technology assessment in health care*, 25(4):514–521, 2009.
- [5] Deborah Hill, Catherine Sarah Holloway, Dafne Zuleima Morgado Ramirez, Peter Smitham, and Yannis Pappas. What are user perspectives of exoskeleton technology? a literature review. *International journal of technology assessment in health care*, 33(2):160–167, 2017.
- [6] Anders Fougnier, Øyvind Stavdahl, Peter J Kyberd, Yves G Losier, and Philip A Parker. Control of upper limb prostheses: Terminology and proportional myoelectric control—a review. *IEEE Transactions on neural systems and rehabilitation engineering*, 20(5):663–677, 2012.
- [7] Elaine Biddiss and Tom Chau. Upper-limb prosthetics: critical factors in device abandonment. *American journal of physical medicine & rehabilitation*, 86(12):977–987, 2007.

- [8] Betsy Phillips and Hongxin Zhao. Predictors of assistive technology abandonment. *Assistive technology*, 5(1):36–45, 1993.
- [9] Technaid S.L. Robotic Exoskeleton Exo-H3. <https://www.technaid.com/products/robotic-exoskeleton-exo-exoesqueleto-h3/>, 2019. [Online; accessed 04-Dec-2019].
- [10] ETH Zürich Cybathlon. Race Task Description Cybathlon 2020. [https://ethz.ch/content/dam/ethz/special-interest/conference-websites-dam/cybathlon-dam/documents/CYBATHLON\\_Races\\_and\\_Rules.pdf](https://ethz.ch/content/dam/ethz/special-interest/conference-websites-dam/cybathlon-dam/documents/CYBATHLON_Races_and_Rules.pdf), 2019. [Online; accessed 04-Dec-2019].
- [11] Robert Riener. The Cybathlon promotes the development of assistive technology for people with physical disabilities. *Journal of neuroengineering and rehabilitation*, 13(1):49, 2016.
- [12] Mohammadreza Asghari Oskoei and Huosheng Hu. Myoelectric control systems — A survey. *Biomedical Signal Processing and Control*, 2(4):275–294, 2007.
- [13] Aaron M Dollar and Hugh Herr. Lower extremity exoskeletons and active orthoses: challenges and state-of-the-art. *IEEE Transactions on robotics*, 24(1):144–158, 2008.
- [14] Tingfang Yan, Marco Cempini, Calogero Maria Oddo, and Nicola Vitiello. Review of assistive strategies in powered lower-limb orthoses and exoskeletons. *Robotics and Autonomous Systems*, 64:120–136, 2015.
- [15] Guillaume Durandau, Dario Farina, Guillermo Asín-Prieto, Iris Dimbwadyo-Terrer, Sergio Lerma-Lara, Jose L Pons, Juan C Moreno, and Massimo Sartori. Voluntary control of wearable robotic exoskeletons by patients with paresis via neuromechanical modeling. *Journal of neuroengineering and rehabilitation*, 16(1):91, 2019.
- [16] Jean-Charles Ceccato, Mathieu De Sèze, Christine Azevedo, and Jean-René Cazalets. Comparison of trunk activity during gait initiation and walking in humans. *PLoS One*, 4(12):e8193, 2009.
- [17] Christoph Anders, Heiko Wagner, Christian Puta, Roland Grassme, Alexander Petrovitch, and Hans-Christoph Scholle. Trunk muscle activation patterns during walking at different speeds. *Journal of Electromyography and Kinesiology*, 17(2):245–252, 2007.
- [18] Pradeep Shenoy, Kai J Miller, Beau Crawford, and Rakesh PN Rao. Online electromyographic control of a robotic prosthesis. *IEEE transactions on biomedical engineering*, 55(3):1128–1135, 2008.
- [19] Kevin Englehart, Bernard Hudgins, et al. A robust, real-time control scheme for multifunction myoelectric control. *IEEE transactions on biomedical engineering*, 50(7):848–854, 2003.
- [20] He Huang, Fan Zhang, Levi J Hargrove, Zhi Dou, Daniel R Rogers, and Kevin B Englehart. Continuous locomotion-mode identification for prosthetic legs based on neuromuscular-mechanical fusion. *IEEE Transactions on Biomedical Engineering*, 58(10):2867–2875, 2011.
- [21] Reza Boostani and Mohammad Hassan Moradi. Evaluation of the forearm emg signal features for the control of a prosthetic hand. *Physiological measurement*, 24(2):309, 2003.
- [22] Jacob Rosen, Moshe B Fuchs, and Mircea Arcan. Performances of Hill-type and neural network muscle models—toward a myosignal-based exoskeleton. *Computers and Biomedical Research*, 32(5):415–439, 1999.
- [23] Silvia Muceli and Dario Farina. Simultaneous and proportional estimation of hand kinematics from emg during mirrored movements at multiple degrees-of-freedom. *IEEE transactions on neural systems and rehabilitation engineering*, 20(3):371–378, 2011.
- [24] Peng Xia, Jie Hu, and Yinghong Peng. EMG-based estimation of limb movement using deep learning with recurrent convolutional neural networks. *Artificial organs*, 42(5):E67–E77, 2018.
- [25] Shaojie Bai, J Zico Kolter, and Vladlen Koltun. An empirical evaluation of generic convolutional and recurrent networks for sequence modeling. *arXiv preprint arXiv:1803.01271*, 2018.
- [26] Joseph L Betthauser, John T Krall, Shain G Bannowsky, György Lévay, Rahul R Kaliki, Matthew S Fifer, and Nitish V Thakor. Stable Responsive EMG Sequence Prediction and Adaptive Reinforcement with Temporal Convolutional Networks. *IEEE Transactions on Biomedical Engineering*, 2019.
- [27] Panagiotis Tsinganos, Bruno Cornelis, Jan Cornelis, Bart Jansen, and Athanassios Skodras. Improved Gesture Recognition Based on sEMG Signals and TCN. In *ICASSP 2019-2019 IEEE International Conference on Acoustics, Speech and Signal Processing (ICASSP)*, pages 1169–1173. IEEE, 2019.
- [28] Adam Hartwell, Visakan Kadirkamanathan, and Sean R Anderson. Compact deep neural networks for computationally efficient gesture classification from electromyography signals. In *2018 7th IEEE International Conference on Biomedical Robotics and Biomechatronics (Biorob)*, pages 891–896. IEEE, 2018.
- [29] Daniel Holden, Taku Komura, and Jun Saito. Phase-functioned neural networks for character control. *ACM Transactions on Graphics (TOG)*, 36(4):42, 2017.
- [30] Sebastian Starke, He Zhang, Taku Komura, and Jun Saito. Neural state machine for character-scene interactions. *ACM Transactions on Graphics (TOG)*, 38(6):1–14, 2019.
- [31] Andrei A Rusu, Mel Vecerik, Thomas Rothörl, Nicolas Heess, Razvan Pascanu, and Raia Hadsell. Sim-to-real robot learning from pixels with progressive nets. *arXiv preprint arXiv:1610.04286*, 2016.
- [32] Samuel Barrett, Matthew E Taylor, and Peter Stone. Transfer learning for reinforcement learning on a physical robot. In *Ninth International Conference on Autonomous Agents and Multiagent Systems-Adaptive Learning Agents Workshop (AAMAS-ALA)*, volume 1, 2010.
- [33] Jose L Contreras-Vidal, Atilla Kilicarslan, He Helen Huang, and Robert G Grossman. Human-centered design of wearable neuroprostheses and exoskeletons. *AI Magazine*, 36(4):12–22, 2015.

- [34] Martín Abadi, Paul Barham, Jianmin Chen, Zhifeng Chen, Andy Davis, Jeffrey Dean, Matthieu Devin, Sanjay Ghemawat, Geoffrey Irving, Michael Isard, et al. Tensorflow: A system for large-scale machine learning. In *12th {USENIX} Symposium on Operating Systems Design and Implementation ({OSDI} 16)*, pages 265–283, 2016.
- [35] François Chollet et al. Keras. <https://keras.io>, 2015. [Online; accessed 10-Jan-2020].
- [36] Guido Rossum. Python reference manual, 1995.
- [37] USA Delsys Incorporated. Delsys trigono, 2019.
- [38] Vicon Motion Systems Ltd. Vicon nexus documentation. <https://docs.vicon.com/display/Nexus29>, 2019. [Online; accessed 10-Jan-2020].
- [39] Christopher L Vaughan, Brian L Davis, and Jeremy C O’connor. *Dynamics of human gait*, volume 2. Human Kinetics, 1992.
- [40] Edward S Grood and Wilfredo J Suntay. A joint coordinate system for the clinical description of three-dimensional motions: application to the knee. *Journal of biomechanical engineering*, 105(2):136–144, 1983.
- [41] Ping Zhou, Blair Lock, and Todd A Kuiken. Real time ECG artifact removal for myoelectric prosthesis control. *Physiological measurement*, 28(4):397, 2007.
- [42] Janessa DM Drake and Jack P Callaghan. Elimination of electrocardiogram contamination from electromyogram signals: An evaluation of currently used removal techniques. *Journal of electromyography and kinesiology*, 16(2):175–187, 2006.
- [43] C Marque, C Bisch, R Dantas, S Elayoubi, V Brosse, and C Perot. Adaptive filtering for ECG rejection from surface EMG recordings. *Journal of electromyography and kinesiology*, 15(3):310–315, 2005.
- [44] Sylvester McGinn and Paul D White. The duration of the qrs complex in the normal and in the abnormal electrocardiogram: A study of 500 cases, with a note on nomenclature. *American Heart Journal*, 9(5):642–654, 1934.
- [45] Günter Klambauer, Thomas Unterthiner, Andreas Mayr, and Sepp Hochreiter. Self-normalizing neural networks. In *Advances in neural information processing systems*, pages 971–980, 2017.
- [46] Sinno Jialin Pan and Qiang Yang. A survey on transfer learning. *IEEE Transactions on knowledge and data engineering*, 22(10):1345–1359, 2009.
- [47] Bernard Widrow, Philippe Baudrenghien, Martin Vetterli, and P Titchener. Fundamental relations between the lms algorithm and the dft. *IEEE Transactions on Circuits and Systems*, 34(7):814–820, 1987.
- [48] K Mayyas and Tyseer Aboulnasr. Leaky lms algorithm: Mse analysis for gaussian data. *IEEE Transactions on Signal Processing*, 45(4):927–934, 1997.
- [49] Thomas G Dietterich. Approximate statistical tests for comparing supervised classification learning algorithms. *Neural computation*, 10(7):1895–1923, 1998.
- [50] Ying-Sheng Luo, Jonathan Hans Soeseno, Trista Pei-Chun Chen, and Wei-Chao Chen. Carl: Controllable agent with reinforcement learning for quadruped locomotion. *ACM Transactions on Graphics (Proceedings of SIGGRAPH 2020)*, 39(4), 2020.
- [51] Kevin Bergamin, Simon Clavet, Daniel Holden, and James Richard Forbes. Drecon: data-driven responsive control of physics-based characters. *ACM Transactions on Graphics (TOG)*, 38(6):1–11, 2019.

# Appendices

## A. Joint Coordinate System

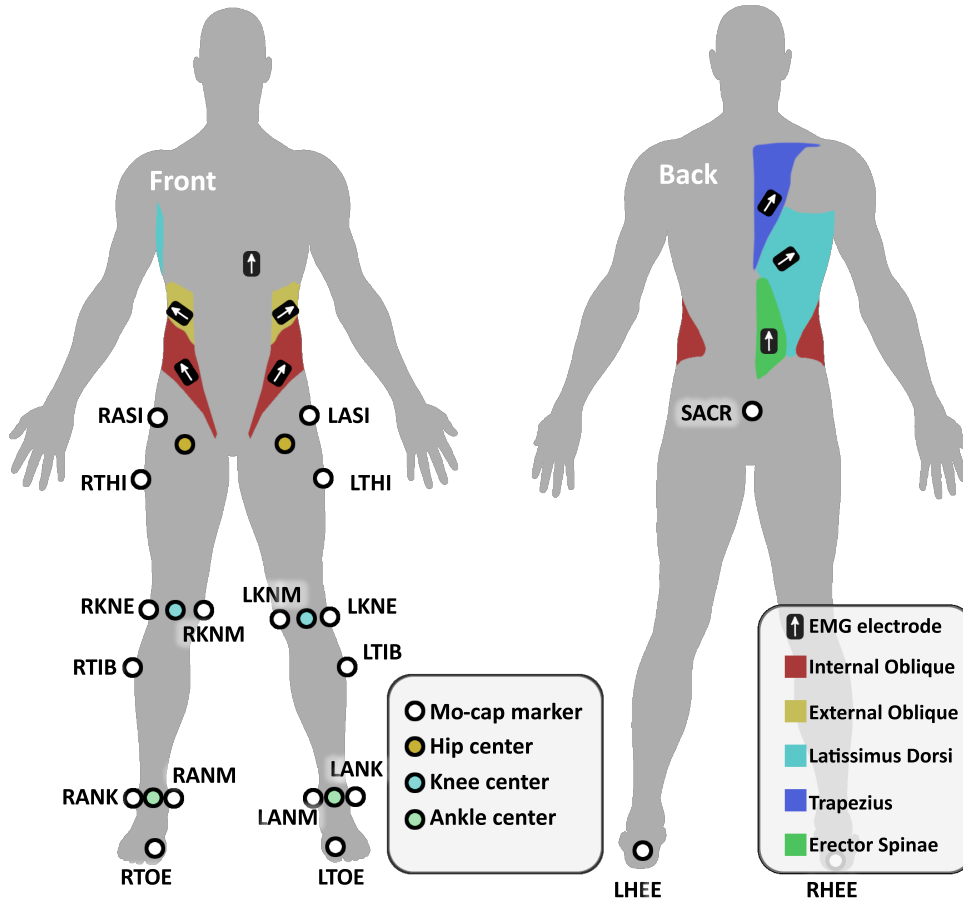


Figure 11. Recording setup for data collection.

Segment	i	j	k
Pelvis	$\overrightarrow{P_{LASI}P_{RASI}}$	$\mathbf{k} \times \mathbf{i}$	$\overrightarrow{P_{SACR}P_{LASI}} \times \overrightarrow{P_{SACR}P_{LASI}}$
Thigh	$\mathbf{j} \times \mathbf{k}$	$\pm \mathbf{k} \times \overrightarrow{P_{HC}P_{THI}}$	$\overrightarrow{P_{KC}P_{HC}}$
Shank	$\mathbf{j} \times \mathbf{k}$	$\pm \mathbf{k} \times \overrightarrow{P_{KC}P_{TIB}}$	$\overrightarrow{P_{AC}P_{KC}}$
Foot	$\mathbf{j} \times \mathbf{k}$	$\pm \mathbf{k} \times \overrightarrow{P_{AC}P_{HEE}}$	$\overrightarrow{P_{TOE}P_{HEE}}$

Table 1. Body segment relative coordinate system definitions. The thigh, shank and foot segments use markers corresponding to their own side (i.e.  $P_{ANK}$  is  $P_{RANK}$  for the right foot). For the  $\mathbf{j}$  vector + is used for the right leg, - for the left leg. Joint center markers referred to as  $P_{HC}$ ,  $P_{KC}$ ,  $P_{AC}$  for the Hip, Knee and Ankle centres respectively

## B. ECG corruption

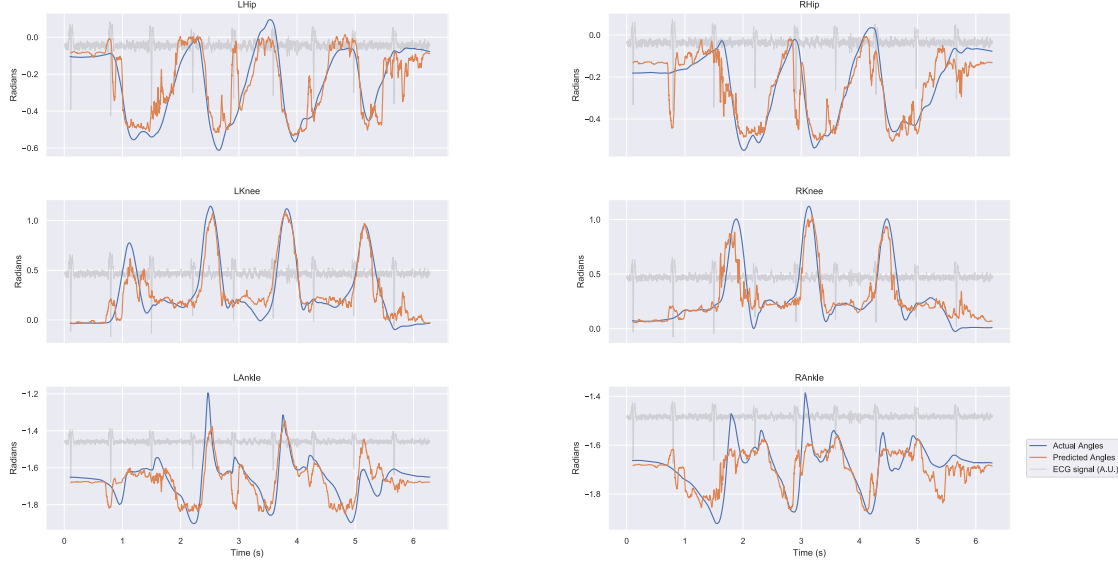


Figure 12. Prediction with a model that uses 100 ms windows. Note the strong correlation between heartbeats and spikes in errors of the hip angles. A 10 ms causal moving average filter has been applied as a postprocessing step.

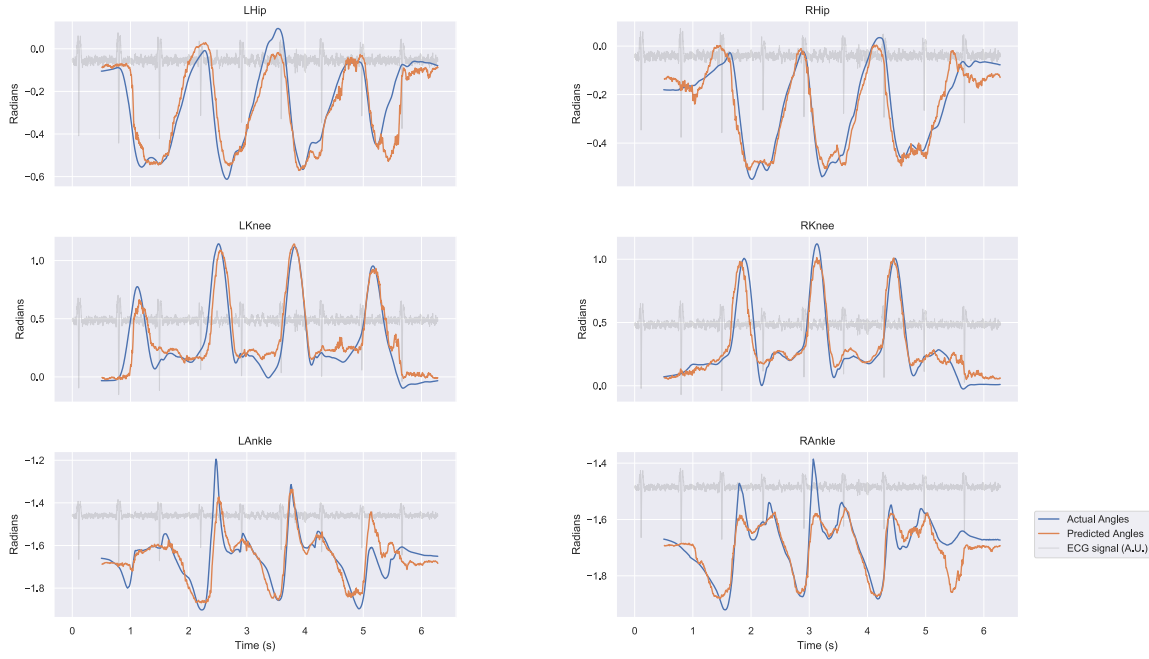


Figure 13. Prediction with a model that uses 500 ms windows. Note less general variability along the absence of the ECG error spikes. A 10 ms causal moving average filter has been applied as a postprocessing step.

### C. Step overshoot

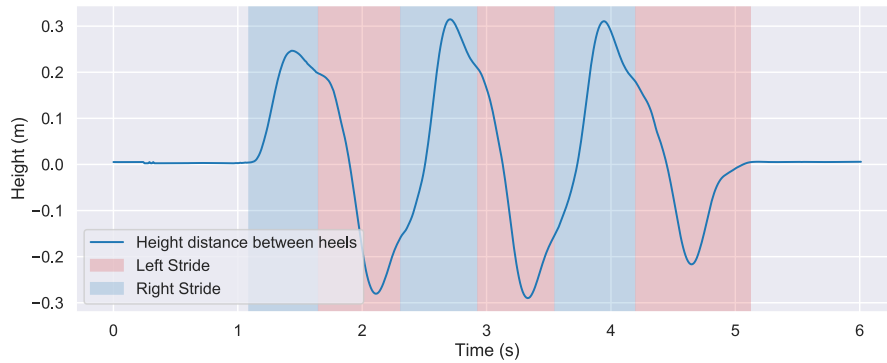


Figure 14. The z coordinate of the right heel - the z coordinate of the left heel plotted for stair ascension. Note the peak distance being before a step is over, which results in greater range of motion in the hips.

## D. NLMS filter

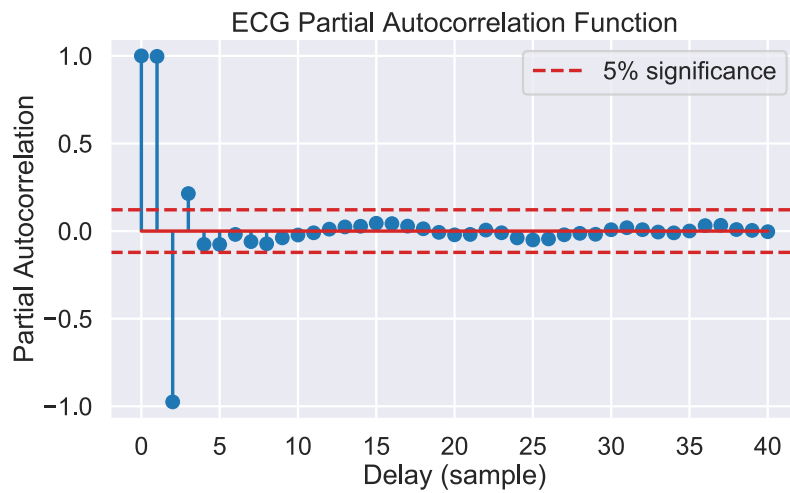


Figure 15. Average partial autocorrelation of the QRS complex with 150ms window. Since adaptive noise cancelling can have 0 delay, filter order of 4 was chosen.

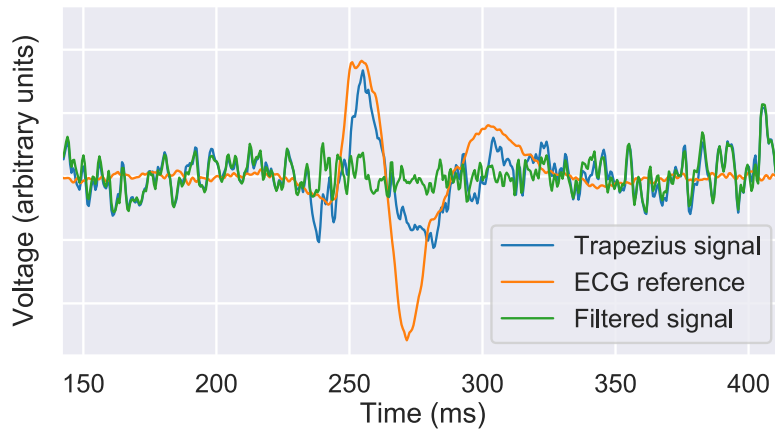


Figure 16. Noise cancellation on Subject 5's trapezius signal.

## E. Regression with spectrum

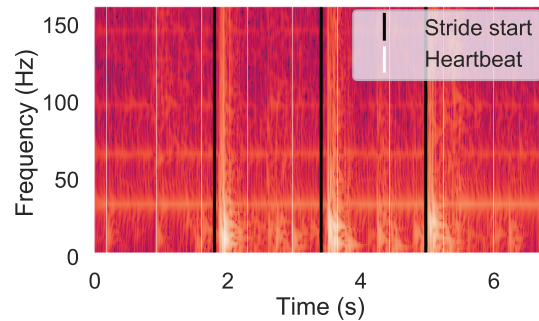


Figure 17. Iterative spectrum estimation of the *erector spinae*. Black bars mark the starts of strides with the right leg; note the muscle's selectivity to it. White bars mark the heartbeats, observable in the 35 Hz region.

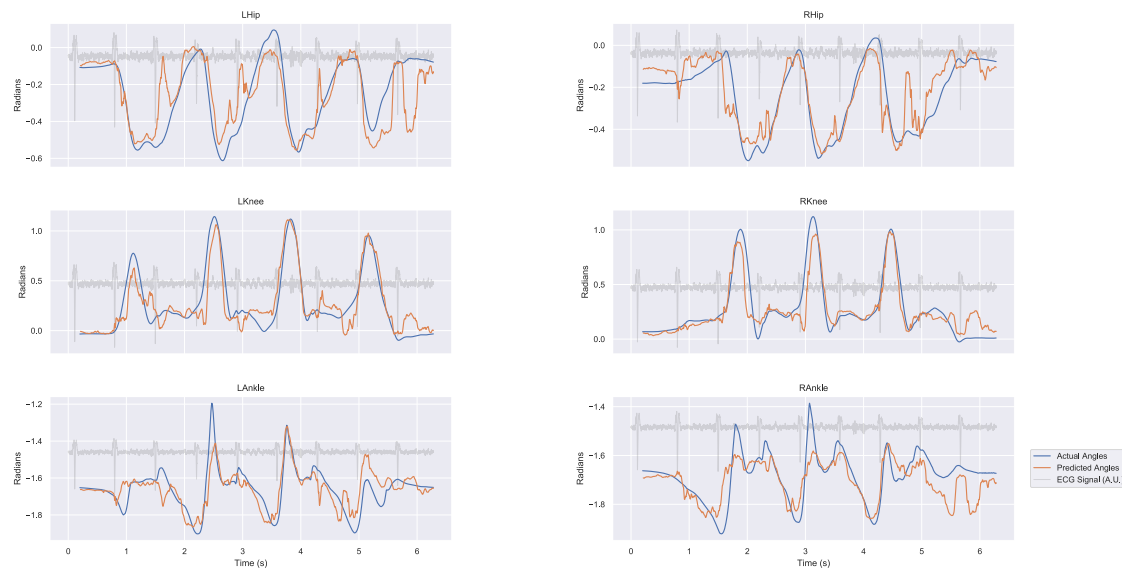


Figure 18. Regression using a 200 ms long window of the spectrum, downsampled 10 fold to reduce dimensionality.